Pergamon

Geochimica et Cosmochimica Acta, Vol. 63, No. 7/8, pp. 1249–1262, 1999

0016-7037/99 $20.00 + .00

PII S0016-7037(99)00015-0

# New lithologies in the Zagami meteorite: Evidence for fractional crystallization of a single magma unit on Mars

T. J. McCoy,[1,2,3,*] M. Wadhwa,[4,5] and K. Keil[1,6]

[1]Hawaii Institute of Geophysics and Planetology, University of Hawaii at Manoa, Honolulu, Hawaii 96822, USA
[2]Code SN4, NASA/Johnson Space Center, Houston, Texas 77058, USA
[3]Department of Mineral Sciences, MRC 119, National Museum of Natural History, Smithsonian Institution, Washington, DC 20560, USA
[4]McDonnell Center for the Space Sciences and Department of Earth and Planetary Sciences, Washington University, St. Louis, Missouri 63130, USA
[5]Department of Geology, The Field Museum, Roosevelt Rd. at Lake Shore Dr., Chicago, Illinois 60605, USA
[6]Hawaii Center for Volcanology, University of Hawaii, Honolulu, HI 96822

(*Received November* 5, 1997; *accepted in revised form January* 8, 1999)

**Abstract**—Zagami consists of a series of increasingly evolved magmatic lithologies. The bulk of the rock is a basaltic lithology dominated by pigeonite ($Fs_{28.7–54.3}$), augite ($Fs_{19.5–35.0}$) and maskelynite ($Ab_{42–53}$). Approximately 20 vol.% of Zagami is a basaltic lithology containing FeO-enriched pyroxene (pigeonite, $Fs_{27.0–80.8}$) and mm- to cm-sized late-stage melt pockets. The melt pockets are highly enriched in olivine-bearing intergrowths, mesostases, phosphates (both whitlockite and water-bearing apatite), Fe,Ti-oxides and sulfides. The systematic increases in abundances of late-stage phases, Fs and incompatible element (e.g., Y and the REEs) contents of pigeonite, Ab contents of maskelynite, and FeO concentrations of whitlockite all point to a fractional crystallization sequence.

The crystallization order in Zagami and the formation of these various lithologies was controlled by the abundances of iron, phosphorus, and calcium. During fractional crystallization, iron and phosphorus enrichment occurred, ultimately forcing the crystallization of calcium phosphates and olivine-bearing intergrowths. The limited amount of calcium in the melt and its partitioning between phosphates and silicates controlled the crystallization of phosphates, plagioclase, pigeonite, and augite. The presence of these FeO-enriched, water-poor late-stage lithologies has important implications. Discrepancies between experimental and petrologic studies to infer the history of basaltic shergottites may be partially explained by the use of starting compositions which are too FeO-poor in the experimental studies. The water-poor nature of the late-stage melt pockets suggests crystallization from a very dry magma, although whether this magma was always dry or experienced significant near-surface degassing remains an open question. Finally, the presence of fractional crystallization products within Zagami suggests that this may be a relatively common process on Mars. 

## 1. INTRODUCTION

Martian (SNC) meteorites provide our only opportunity to study the products of Martian magmatic processes in our laboratories. These meteorites provide a mechanism to unravel both the early differentiation history of Mars and the physical and chemical processes acting during more recent (1.3 Ga to present) events. Differences between these meteorites detail the range of igneous processes occurring on Mars. Elephant Moraine A79001 was the first Martian meteorite documented to contain large-scale heterogeneity (McSween and Jarosewich, 1983), providing important clues to the processes occurring within individual magma units. In this work, we demonstrate that Zagami also is heterogeneous on a large scale, and that study of the diverse lithologies can provide insights into the magmatic processes occurring during its crystallization.

The Zagami meteorite fell as a single stone of ~18 kg in Nigeria in 1962. It is a fine- to medium-grained rock of basaltic composition and one of the basaltic shergottites, a group which includes Shergotty, EET A79001, QUE 94201 and Dar al Gani 476. Stolper and McSween (1979) provided a comprehensive petrologic and experimental study of the small amount of material (~250 g) from Zagami available at the time. In 1988, the main mass of this meteorite became available for study, stimulating work by Treiman and Sutton (1992) and McCoy et al. (1992). Even these studies demonstrated only minor differences (e.g., grain size, oxide abundances) between different pieces of Zagami. In 1992, Vistisen et al. (1992) documented the existence of a cm-sized olivine-rich sample of Zagami, suggesting that a more thorough study of all available material might provide additional clues to the genesis of this important Martian rock (McCoy et al., 1993; Wadhwa et al., 1993).

We report here the results of an extensive petrologic and geochemical study of Zagami. The rock exhibits a range of lithologies that become increasingly enriched in iron oxide and incompatible elements (e.g., P, Ti, Zr, and REEs). These lithologies range from the basaltic lithology studied by Stolper and McSween (1979) to late-stage melt pockets that are highly enriched in phosphates, mesostases, sulfides, and oxides. We suggest these lithologies formed through extensive fractional crystallization of the magma unit of which Zagami is a sample. The type of differentiation observed in this meteorite may have occurred commonly in magma bodies on Mars.

*Author to whom correspondence should be addressed (USA mccoy.tim@nmnh.si.edu).

## 2. SAMPLES AND TECHNIQUES

We studied multiple samples of Zagami, examined each under the binocular microscope, photographed each piece and prepared thin sections of appropriate materials. Robert Haag provided access to ~5.2 kg of Zagami with a sawn surface area of ~910 $cm^2$. Polished thin sections UH 217 and 218 were prepared from this material. Access to a 442 gram sample (USNM 6545) and polished thin section (USNM 6545-1) was provided by the Smithsonian Institution. Lise Vistisen and colleagues provided material from a large, late-stage melt pocket and we prepared two polished thin sections (UH 233, 234) from this material. UH sections are deposited in the collection of the Hawaii Institute of Geophysics and Planetology.

All thin sections were examined in reflected and transmitted light. Phase analyses were conducted with Cameca Camebax and Cameca SX-50 electron microprobes. For analyses of pyroxene and olivine, a 1-$\mu$m beam and 15-nA current were used, whereas analyses of maskelynite, mesostases, and phosphates utilized a 10-nA current and 5- to 10-$\mu$m beam size to reduce volatile loss. Well-known standards were used. Concentrations of REEs and other selected trace and minor elements were measured in situ in various minerals present in sections of the late-stage melt pockets (UH 233) and the dark, mottled lithology (UH 217, 218) with the Washington University modified CAMECA IMS-3f ion microprobe. Experimental techniques for ion microprobe analyses are described in detail by Zinner and Crozaz (1986) and Lundberg et al. (1988).

## 3. RESULTS

Zagami consists of a series of increasingly evolved magmatic lithologies. The bulk of the rock (termed normal Zagami, ~80 vol.%) is the basaltic lithology studied by Stolper and McSween (1979), McCoy et al. (1992), Treiman and Sutton (1992) and Wadhwa et al. (1994). The remaining ~20 vol.% is a basaltic lithology that is enriched in FeO, has a heterogeneous distribution of pyroxene and maskelynite on a mm-scale, and was termed the dark, mottled lithology by McCoy et al. (1995). It contains mm- to cm-sized late-stage melt pockets that are highly enriched in olivine, $SiO_2$, phosphates, Fe, Ti-oxides, and sulfides (Vistisen et al., 1992; McCoy et al., 1993). These pockets make up ~10 vol.% of the dark, mottled lithology, or ~2 vol.% of the rock. The largest of these pockets was termed the DN lithology by Vistisen et al. (1992). We do not use the DN nomenclature in this article, but do present data from this material because it is the largest, most evolved late-stage melt pocket from the Zagami material studied by us. Shock-melt veins and pockets are also present in Zagami and have previously been discussed by McCoy et al. (1992) and Marti et al. (1995).

### 3.1. Textures

The complete range of lithologies known to exist in Zagami have been observed in two samples from the Haag collection (a 1.85 kg part slice and a 2.78 kg end piece) and in the 442 g sample from the Smithsonian (USNM 6545) and, therefore, spatial associations can be observed (Figs. 1a–c). The bulk of the samples are composed of normal Zagami and are light-colored and fine grained. The FeO-rich lithology is darker in color and mottled in appearance. These two lithologies are separated by a reasonably sharp, although not necessarily straight, contact (Figs. 1a,c). Finally, within the dark, mottled lithology occur the late-stage melt pockets that range in size from a few hundred microns to more than a cm in diameter.

The dark, mottled lithology (Fig. 2a) is generally similar to normal Zagami in mineralogy and texture and consists mostly of a homogeneous mixture of maskelynite and pyroxene. Amphiboles, although observed in only four melt inclusions in three separate pyroxene grains in this lithology, occur in the Mg-rich cores of pyroxenes, as is also the case in normal Zagami (McCoy et al., 1992). Grain sizes (0.24–0.31 mm) of

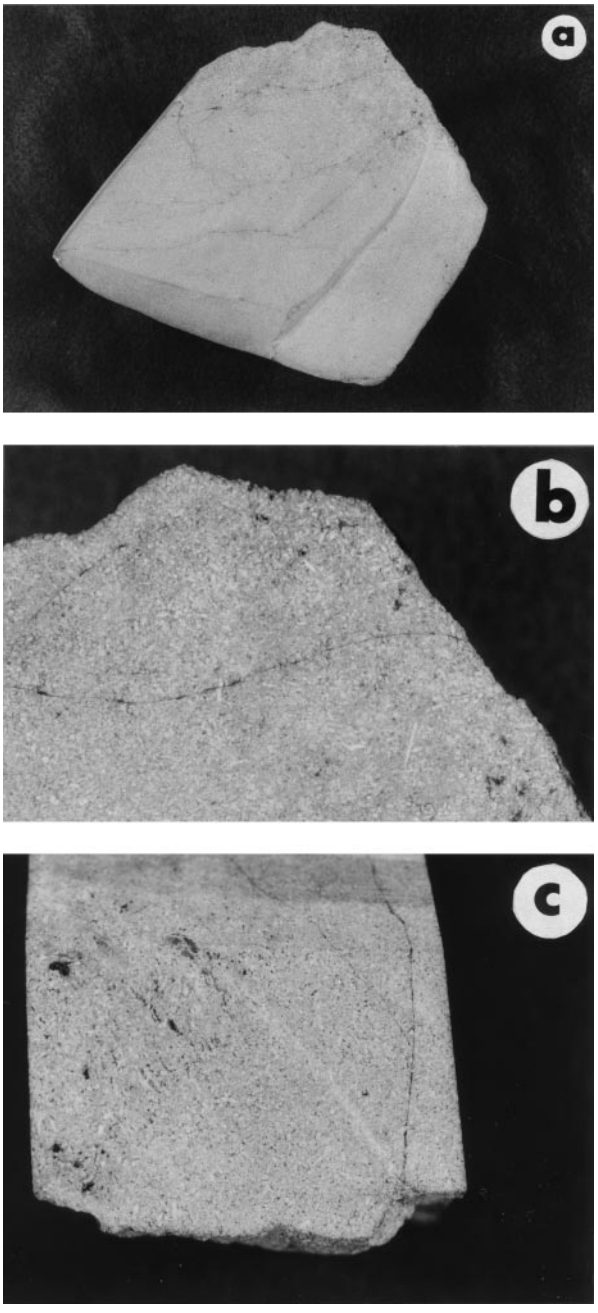


Fig. 1. Hand sample photographs of Zagami. (a) Cut face of a 2.78 kg end piece with dark, mottled lithology at the top and normal Zagami at the bottom. Shock-melt veins cross-cut the specimen. Width = 18 cm. (b) Close-up view of the dark, mottled lithology. Field of view is 7 cm. (c) Sample USNM 6545 (~5 cm across) with the dark, mottled lithology (upper left) separated from normal Zagami (lower right) by a planar contact. The dark, mottled lithology contains late-stage melt pockets, impact-melt pockets, and elongate maskelynite.

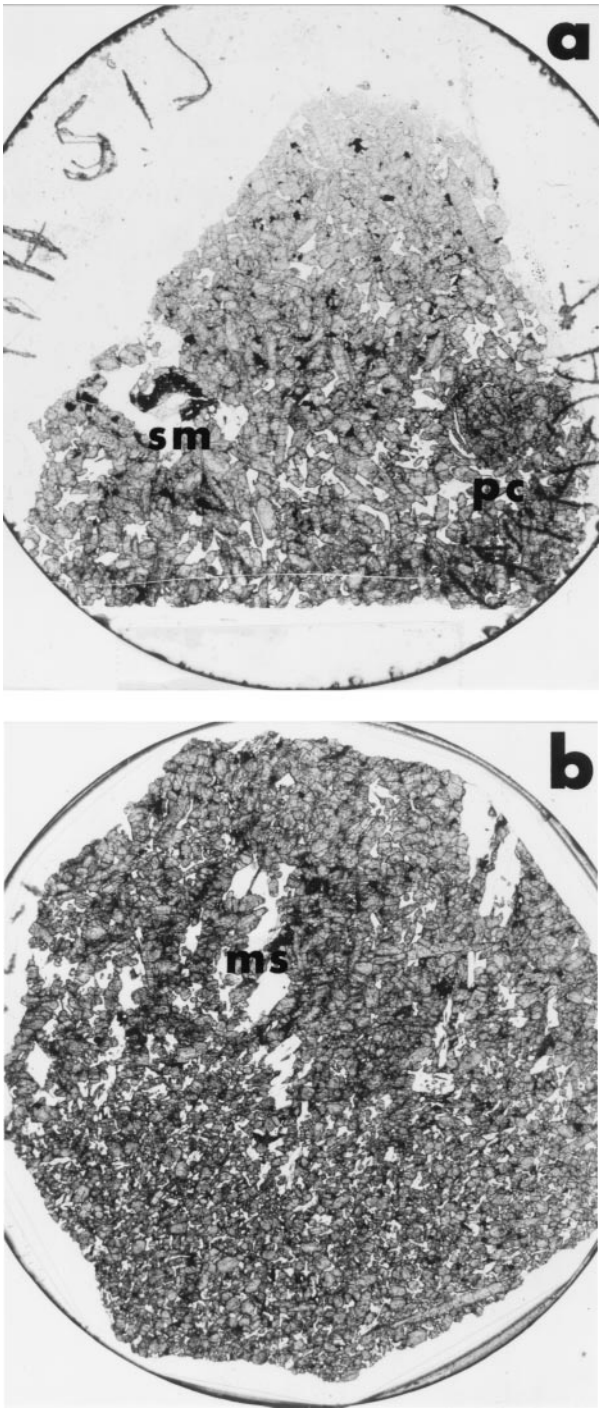


Fig. 2. (a) Polished thin section (UH 217) of the dark, mottled lithology. Prominent features include a large shock-melt pocket (sm) and a pyroxene clump (pc). (b) PTS USNM 6545-1, with the dark, mottled lithology at the top and normal Zagami at the bottom, separated by a planar contact. Prominent in the dark, mottled lithology are the elongate maskelynite stringers (ms). Sections are 2.6 cm in diameter.

the dark, mottled lithology are comparable to those of normal Zagami (0.17–0.36 mm; McCoy et al., 1992). However, unlike normal Zagami, minerals in the dark, mottled lithology do not exhibit a preferred alignment (using the method of Darot, 1973). It also differs from normal Zagami in containing mm-sized areas substantially enriched in pyroxene or plagioclase. In all sections of the dark, mottled lithology, pyroxene clumps up to ~4 mm in diameter are found (Fig. 2a). The centers of these clumps typically contain FeO-rich pyroxene, are depleted in maskelynite and are enriched in phosphates, Fe, Ti-oxides, pyrrhotite, and mesostasis (Fig. 3). We also observed stringers of large (up to 3 mm) maskelynite grains that originate at the boundary between the dark, mottled lithology and normal Zagami and are oriented perpendicular to this boundary (Fig. 2b).

The smallest of the late-stage melt pockets in the dark, mottled lithology are similar mineralogically to those in normal Zagami (Stolper and McSween, 1979) and contain mesostases, phosphates, Fe-Ti oxides, and pyrrhotite. The largest of these melt pockets, typified by the Vistisen et al. (1992) sample, occur within the pyroxene clumps and contain pyroxene, maskelynite, Fe,Ti oxides, pyrrhotite, whitlockite, and rare apatite as mm-sized phenocrysts; abundant mesostases and fayalite-bearing intergrowths are also present. The largest such late-stage melt pocket contains only 13.6% pyroxenes (mostly pigeonite; augite is absent as a phenocryst phase but is present within the fayalite-bearing intergrowths), far less than the 70–80% typical of the rest of Zagami (Fig. 4a,b; Table 1). Phases that are normally found in minor abundances ($<$ 3%) in normal Zagami are prominent in this pocket, including Fe,Ti-oxides (5.9%), pyrrhotite (1.6%), and phosphates (11.4%). Apart from these phenocryst phases, this largest melt pocket is composed of a diverse set of intergrowths. Adjacent to the pigeonite phenocrysts occur a vermicular intergrowth of augite, fayalite and a silica-rich material (probably $SiO_2$ + maskelynite + K-feldspar) (Fig. 5a). Adjacent to large phosphate grains, fayalite occurs with wormy inclusions of $SiO_2$ + maskelynite + K-feldspar ± whitlockite ± Fe,Ti oxides ± sulfides (Fig. 5b). Fayalite comprises 25–50 vol.% of these two intergrowths. Mesostases are composed of maskelynite + $SiO_2$ ± K-feldspar. The K-rich mesostases tend to be finer-grained than the K-poor variety. Late-crystallizing mesostases, Fe,Ti-oxides and pyrrhotite can all occur as mm-sized particles.

### 3.2. Major Element Mineral Compositions

Pigeonites in normal Zagami range in composition from $Fs_{28.7}Wo_{15.4}$ to $Fs_{54.3}Wo_{9.7}$, whereas augites range from $Fs_{19.5}Wo_{34.4}$ to $Fs_{35.0}Wo_{32.7}$ (McCoy et al., 1992; McCoy, unpublished data). Pigeonites in the dark, mottled lithology and its late stage melt pockets exhibit a very broad range of compositions ($Fs_{27.0-80.8}$), as do the augites ($Fs_{19.3-56.2}$); note that these compositions range to much higher FeO concentrations than those in normal Zagami (Fig. 6; Table 2). The most FeO-enriched grains always occur in the centers of the late-stage melt pockets, where Mg-rich pyroxenes are absent (Fig. 3). The largest late-stage melt pocket contains pigeonites with compositions from $Fs_{56.0}Wo_{23.6}$ to $Fs_{70.7}Wo_{11.3}$, substantially enriched in FeO relative to normal Zagami. Augite is not a phenocryst phase in this melt pocket, but does occur within fayalite-bearing intergrowths ($Fs_{46.6-53.6}$) and as isolated grains in the mesostases ($Fs_{53.2-56.2}Wo_{40.3-42.0}$; Table 2, Fig. 6).

Maskelynite compositions in normal Zagami range from

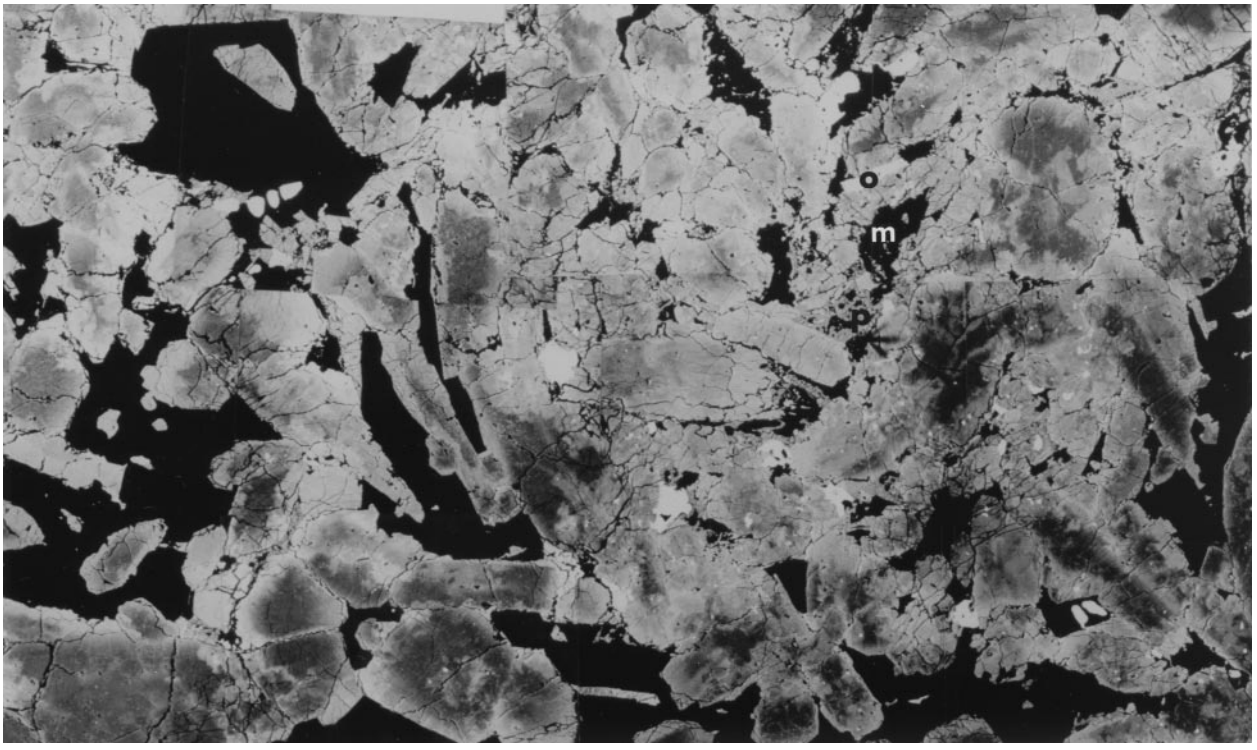


Fig. 3. BSE photomosaic of the pyroxene clump from Fig. 2a. Pyroxenes in the center of the clump are highly enriched in FeO compared to those on the edges. Opaques (o), phosphates (p), and mesostases (m) are abundant in the center of the clump. Field of view is ~7.5 mm.

$Ab_{42-53}Or_{1-4}$ (Stolper and McSween, 1979). Maskelynite in the dark, mottled lithology and its late-stage melt pockets ($Ab_{50.2-58.8}$; Fig. 7, Table 3) overlaps with this range and extends it to more sodic compositions. Maskelynite phenocrysts in the largest late-stage melt pocket lie towards the sodic end of this range ($Ab_{56.0-58.8}$).

Zagami contains a variety of mesostasis materials in late-stage melt pockets, which appear to be mixtures of plagioclase + $SiO_2$ ± K-feldspar or shock-produced glasses of these three phases (Stolper and McSween, 1979). Potassium-poor mesostasis occurs as pockets up to a millimeter in size and in the fayalite-bearing intergrowths. Individual analyses of the K-poor mesostasis (Table 4) vary significantly in their normative quartz abundances and exhibit a range in feldspar composition (calculated from the abundances of $Na_2O$, CaO and $K_2O$ and normalized to 100%). The K-poor mesostasis appears to be a mixture of $SiO_2$, which comprises 0–91.4 normative % of individual analyses, and maskelynite. The maskelynite component ranges in composition from $Ab_{58.3}Or_{4.0}$ to $Ab_{72.6}Or_{2.7}$ (Table 4), consistently more albitic than maskelynite phenocrysts in the dark, mottled lithology (Fig. 7). Potassium-rich mesostasis occurring both as large pockets and in the fayalite intergrowths have comparable ranges of compositions, scattering in an array from orthoclase-rich (up to $Ab_{22.6}Or_{72.7}$) toward the composition of the K-poor mesostasis, reaching $Ab_{76.0}Or_{18.0}$ (Fig. 7). The majority of analyses fall in the range $An_{3-16}Or_{57-73}$, with normative quartz ranging from 30–42% (Table 4, Fig. 7). These compositions suggest that the K-rich mesostases is a mixture of $SiO_2$, maskelynite and K-feldspar.

Phosphates are abundant in late-stage melt pockets of all sizes. In the largest of these, phosphates comprise 11.4 vol.%. Although both whitlockite and apatite occur in the melt pockets, the former is by far the more abundant. Whitlockites vary in FeO from 2.65–5.15 wt.% FeO (Table 5), ranging to significantly higher concentrations than found in normal Zagami (2.59–3.47 wt.% FeO; McCoy et al., 1992; McCoy, unpublished data). Not surprisingly, the largest late-stage melt pocket has the most FeO-enriched whitlockites (4.96–5.15 wt.% FeO). Apatite occurs as large phenocrysts and they contain small amounts of FeO, MnO and MgO (Table 5). Stoichiometries calculated on the basis of 12 oxygens consistently reveal a deficiency in F and Cl relative to the ideal value of 1 (Table 5). This deficiency would correspond to the presence of ~0.50 wt.% water. Watson et al. (1994) determined a water content of ~0.3–0.4 wt.% for one of these apatite grains by ion microprobe analysis, confirming the presence of structural pre-terrestrial water.

Fayalite has previously been observed in normal Zagami, with a range of compositions from $Fa_{90-93}$ (Stolper and McSween, 1979). This mineral occurs in fine-grained intergrowths in the late-stage melt pockets, particularly in the largest of these pockets. In one late-stage melt pocket, a fayalite grain 150 $\mu$m in diameter was observed. Fayalite compositions in different textural settings are all FeO-rich and comparable in composition (Table 6), with a range from $Fa_{90.0-96.7}$. Fayalite occurring with FeO-rich phases (e.g., augite, ilmenite) have lower FeO concentrations than those occurring with phosphates.

Stolper and McSween (1979) reported that Fe,Ti oxides in normal Zagami included ilmenite ($Ilm_{95}Hm_5$) and titanomagnetite ($Mt_{37}Usp_{63}$), suggesting crystallization at an ($fO_2$ close

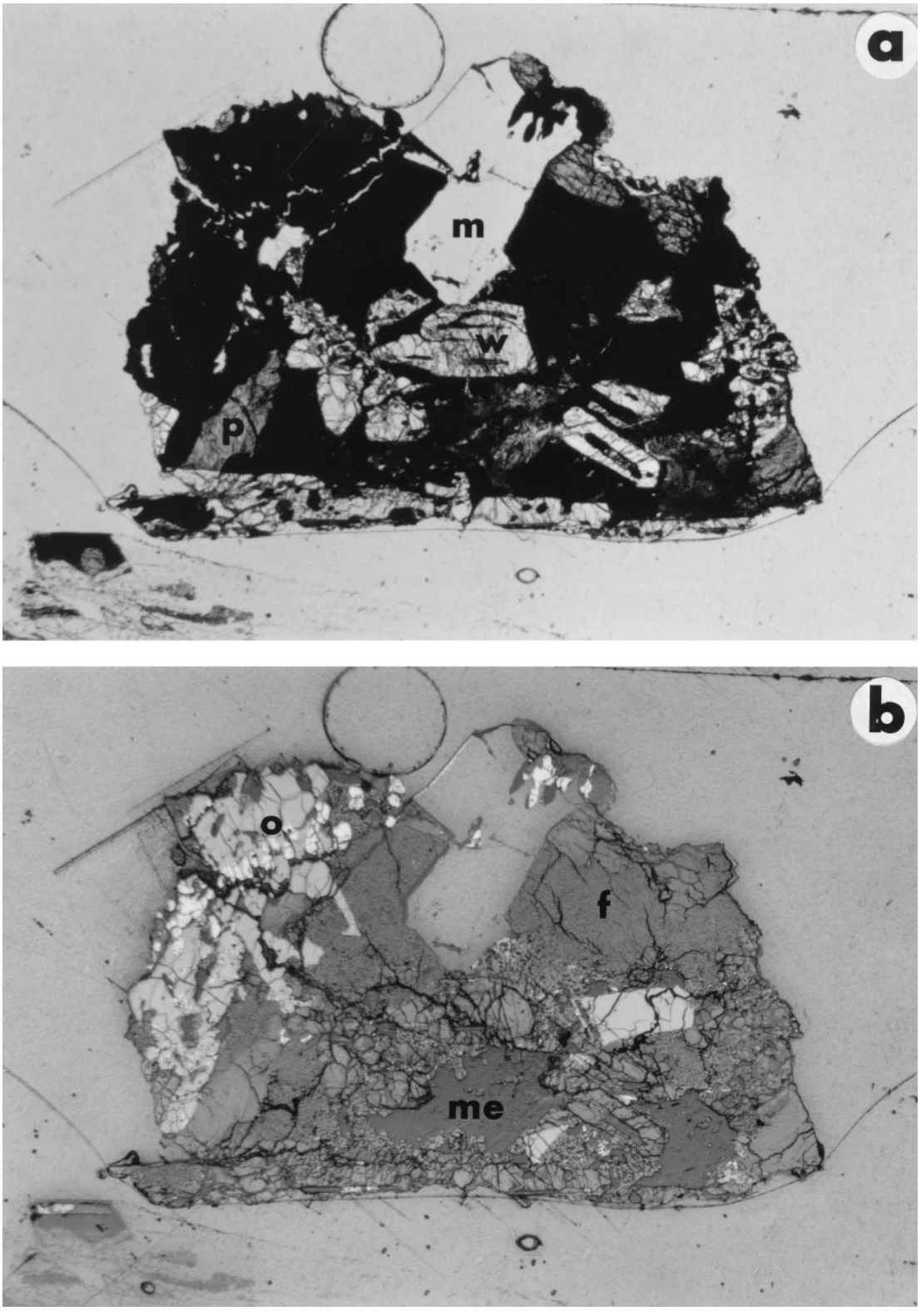


Fig. 4. Photomicrographs of a section of the largest late-stage melt pocket in both transmitted, plane polarized (a), and reflected light (b). Width = 4 mm. (a) Clear maskelynite (m), pigeonite (p), and skeletal whitlockite (w) are the major phenocryst phases. (b) Other phases include Fa-bearing intergrowths (f), the opaques Fe, Ti-oxides, and pyrrhotite (o), and mesostases (me) (both K-rich and K-poor).

Table 1. Modal analyses (vol.%) and average grain sizes of the three magmatic lithologies of Zagami, as obtained by study of polished thin sections.

| | Normal Zagami | | | Dark, mottled lithology | | | Late-stage melts |
|---|---|---|---|---|---|---|---|
| Phase | UNM 991 | UNM 994 | USNM 6545-1 | USNM 6545-1 | UH 217 | UH 28 | UH 233, 234 |
| Pyroxene | 77.1 | 80.4 | 73.6 | 71.3 | 76.9 | 80.3 | 13.6 |
| Maskelynite | 17.6 | 10.3 | 21.4 | 21.6 | 13.6 | 9.3 | 19.0 |
| Mesostasis | 1.8 | 3.7 | 1.7 | 3.3 | 2.9 | 4.1 | 8.1 |
| Fe, Ti-Oxides | 1.5 | 2.6 | 1.7 | 1.3 | 2.6 | 2.6 | 5.9 |
| Pyrrhotite | 0.6 | 0.6 | 0.4 | 0.7 | 0.6 | 0.6 | 1.6 |
| Phosphates | 0.5 | 1.3 | 1.1 | 1.4 | 1.9 | 2.2 | 11.4 |
| Shock melt | 0.1 | 0.9 | — | 0.2 | 1.1 | 0.5 | — |
| Fa Intergrowth | — | — | — | Tr | — | Tr | 39.9 |
| No. of points | 2000 | 2000 | 1054 | 1415 | 1667 | 1942 | 2010 |
| Grain size (mm) | 0.24 | 0.36 | 0.17 | 0.24 | 0.30 | 0.31 | — |
| Alignment | Yes | No | No | No | No | No | — |

—, not present; Tr, <0.1 %.

to the quartz-fayalite-magnetite buffer. These same phases are found in all lithologies of Zagami, and our analyses (Table 7) show only very minor compositional differences between lithologies, with titanomagnetite ranging in composition from $Usp_{63-68}$ and titanomagnetite from $Hm_{4-5}$. The inference that all the lithologies in Zagami crystallized near the QFM buffer is consistent with the presence of $SiO_2$, fayalite and titanomagnetite as major constituents of the late-stage melt pockets. It is interesting to note that while the late-stage melt pockets are similar in degree of fractionation to QUE 94201, the latter formed at much more reducing conditions (McSween et al., 1996). Three pyrrhotite grains in the largest late-stage melt pocket are identical in composition to those of normal Zagami ($Fe_{0.94}S$; Stolper and McSween, 1979).

### 3.3. Trace Element Mineral Compositions

REE *patterns* of the various minerals in the dark, mottled lithology (Table 8, Fig. 8a) are similar to those in normal Zagami (Wadhwa et al., 1994). Low- and high-Ca pyroxenes have the characteristic LREE-depleted patterns (typically somewhat steeper for pigeonite than for augite), with small Eu anomalies (Eu/Eu* ~0.6–0.8, where Eu* is the value interpolated between chondrite-normalized values of Sm and Gd). However, the range of *absolute abundances* of incompatible trace elements in pyroxenes in the dark, mottled lithology is significantly different from that in normal Zagami. Although there is some overlap, pyroxene compositions in the dark, mottled lithology extend to much higher REE and other incompatible element concentrations than those in normal Zagami. This is evident from comparing the compositional range of pigeonites in the dark mottled lithology with that in normal Zagami (Fig. 9).

Maskelynite in the dark, mottled lithology has a LREE-enriched pattern with a strong positive Eu anomaly (Eu/Eu* ~ 60–80). Apatite has a relatively flat REE pattern, with La ~ 15–20 × CI. Whitlockite has the highest REE abundances of all the analyzed minerals and is the main carrier of REEs (as is the case for all shergottites); La abundances are 480–650 × CI in whitlockite in the dark, mottled lithology as compared to 400–480 × CI in whitlockite in normal Zagami. As in the case of whitlockite in normal Zagami (Wadhwa et al., 1994), the REE pattern of this mineral (with the exception of the small Eu anomaly) in the dark, mottled lithology is parallel to that of the Zagami bulk rock.

We also report the trace element compositions of minerals in the largest of the melt pockets (Table 8, Fig. 8b). The range of incompatible trace element abundances in pigeonite of this melt pocket has significant overlap with that in normal Zagami, but extends to somewhat higher concentrations than even the dark, mottled lithology (Fig. 9).

Maskelynite in this largest late-stage melt pocket has a LREE-enriched pattern, with a strong positive Eu anomaly (Eu/Eu* ~ 60–90). Apatite in this pocket has relatively higher REE abundances (La ~ 20–30 × CI) than that typically found in the dark, mottled lithology. Moreover, the REE pattern of this apatite appears to be more fractionated (i.e., HREE depleted and with a more pronounced negative Eu anomaly) than that of apatite in the dark, mottled lithology. REE abundances in whitlockite of this melt pocket (La ~ 500–540 × CI) fall within the range of REE concentrations in whitlockite in the dark, mottled lithology.

## 4. CRYSTALLIZATION HISTORY OF ZAGAMI

The presence of related magmatic lithologies occurring within a single Martian meteorite can help to elucidate the process of differentiation within magma units on Mars. The data presented here and in previous studies (Stolper and McSween, 1979; McCoy et al., 1992; Treiman and Sutton, 1992) suggest that the sequence of normal Zagami to the dark, mottled lithology to the late-stage melt pockets is, by and large, a sequence of progressively increasing fractional crystallization, resulting in the formation of increasingly evolved residual melts (Table 9). The abundance of late-stage phases, most notably fayalite, increases systematically from normal Zagami to the dark, mottled lithology to the late-stage melt pockets, as does the Fs and incompatible element (e.g., Y and the REEs) contents of pigeonite, the Ab contents of maskelynite, and the FeO concentrations of whitlockite. It is noted, however, that the crystallization sequence within the late-stage melt pockets may not necessarily be identical owing to their isolation from each other and local compositional variations within their immediate environments of crystallization.

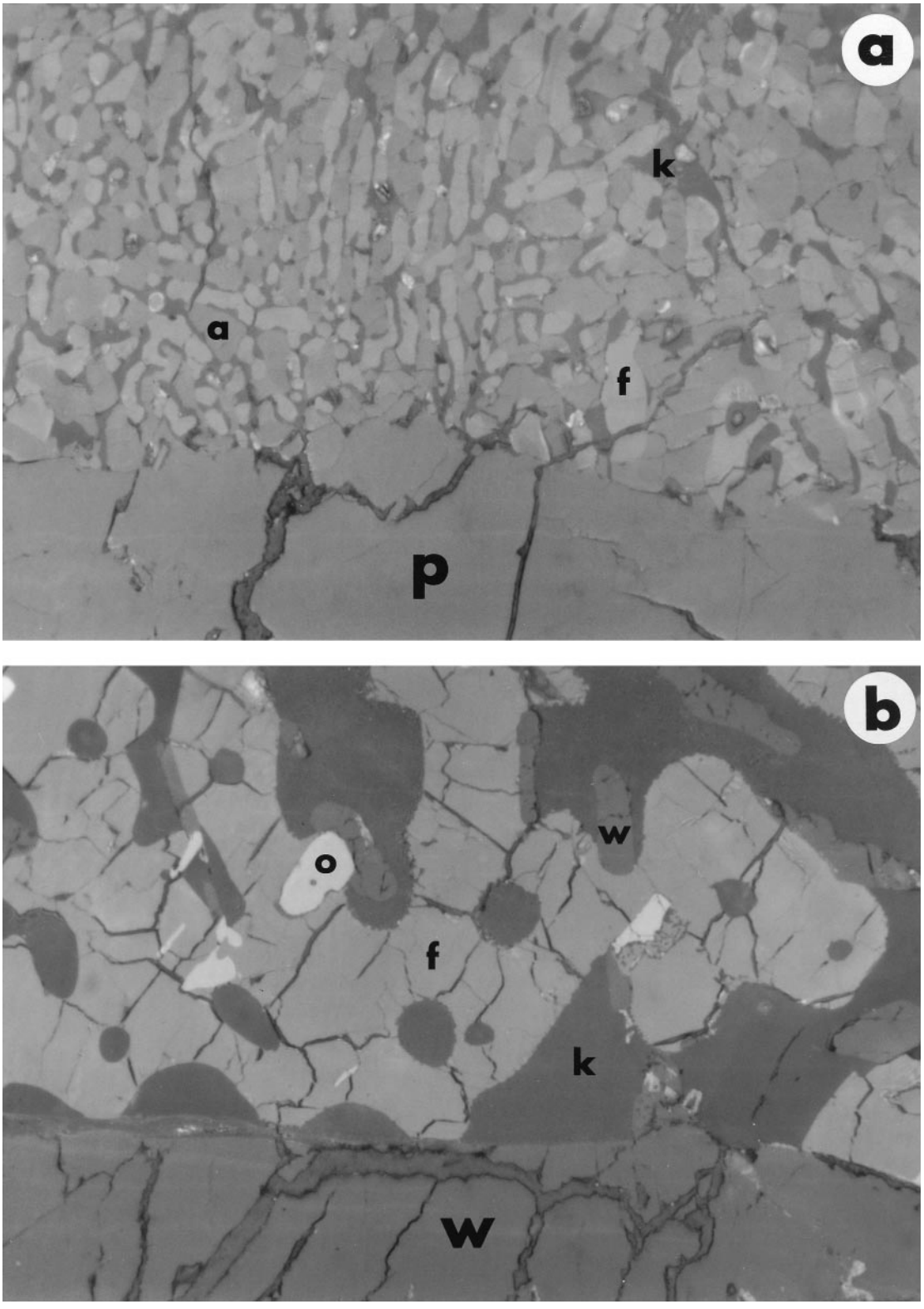


Fig. 5. Reflected light photomicrographs (fields of view = 130 $\mu$m) of late-stage fayalite-bearing intergrowths. (a) Pigeonite phenocrysts (p) bounded by a vermicular intergrowth of augite (a), fayalite (f), and K-rich mesostasis (k). (b) Whitlockite (w) phenocryst bounded by a coarser-grained mixture of fayalite (f), K-rich mesostasis (k), smaller whitlockites (w), and opaque phases (pyrrhotite and Fe,Ti-oxides) (o).

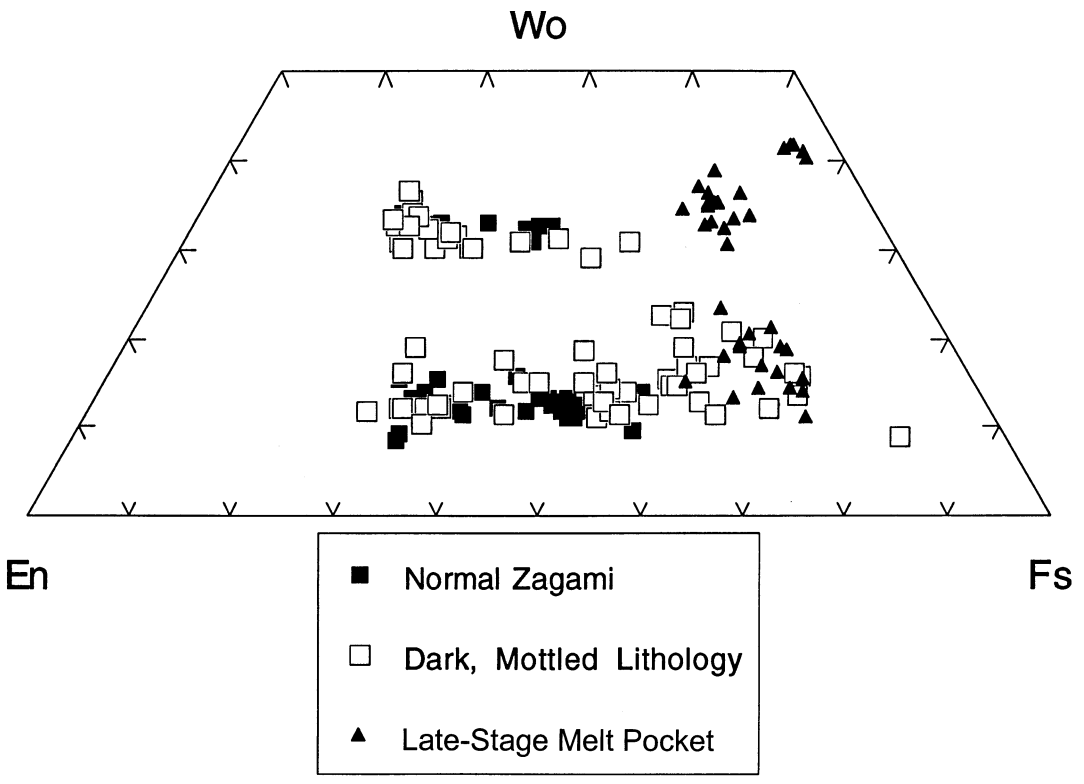


Fig. 6. Pyroxene quadrilateral showing compositions of pyroxenes from normal Zagami (McCoy et al., 1992), the dark, mottled lithology, and the largest late-stage melt pocket. Each lithology contains increasingly FeO-enriched pigeonite, reflecting formation of these lithologies via fractional crystallization.

Considerable debate remains about the crystallization history of Zagami. McCoy et al. (1992) suggested a two-stage magmatic history, where homogeneous Mg-rich pyroxenes crystallizing in a deep-seated (1–2 kbar, 7.5–15 km depth on Mars), slowly-cooling magma chamber, with subsequent emplacement of an ~10-m thick flow, which cooled at <0.5°C/h. Slow cooling was supported by the work of Brearley (1991). In contrast, Treiman and Sutton (1992) inferred a single-stage magmatic history with relatively rapid cooling (2–20°C/h). Since that time, experiments by McCoy and Lofgren (1996) have confirmed the need for slow cooling during crystallization to produce textures similar to those of Zagami. However, measurements of lower than expected water concentrations in the kaersutitic amphibole occurring within melt inclusions in the cores of Mg-rich pyroxenes in Zagami (Watson et al., 1994) and recent experimental work by Popp et al. (1995a,b) suggest that these low-OH kaersutites may be stable at lower pressures, and, therefore, at shallower depth than previously assumed. Whether or not Zagami experienced a period of crystallization at depth, it clearly experienced a period of relatively slow cooling and crystallization in a moderately-thick magma body at or near the surface of Mars. Our new results suggest that significant fractional crystallization occurred during this period.

The crystallization order in Zagami can be inferred from the

Table 2. Representative analyses of pigeonite and augite illustrating the range of variability.

| | Pigeonite | | | | | | | | | Augite | | | | | |
|---|---|---|---|---|---|---|---|---|---|---|---|---|---|---|---|
| | Dark, mottled lithology | | | | | | Late-stage melts | | | Dark, mottled lithology | | | Late-stage melts | | |
| $SiO_2$ | 53.9 | 51.2 | 50.6 | 49.1 | 47.9 | 46.6 | 48.1 | 47.9 | 48.0 | 53.1 | 51.7 | 49.7 | 48.6 | 48.5 | 46.5 |
| $Al_2O_3$ | 0.68 | 1.25 | 0.79 | 0.59 | 0.63 | 0.61 | 0.84 | 0.69 | 0.39 | 0.94 | 1.34 | 0.92 | 0.97 | 0.69 | n.d. |
| FeO | 17.4 | 24.3 | 30.2 | 34.5 | 38.1 | 44.1 | 33.1 | 37.1 | 40.8 | 12.3 | 17.3 | 25.5 | 27.6 | 31.3 | 30.8 |
| MgO | 22.0 | 15.37 | 13.1 | 9.06 | 5.21 | 3.12 | 6.73 | 5.64 | 5.79 | 17.0 | 14.2 | 8.72 | 5.23 | 4.1 | 1.74 |
| CaO | 6.02 | 7.14 | 5.31 | 5.96 | 6.94 | 3.85 | 10.9 | 8.38 | 5.11 | 16.3 | 14.5 | 13.8 | 17.1 | 15.4 | 18.8 |
| Total | 100.11 | 99.23 | 100.06 | 99.17 | 98.69 | 98.28 | 99.67 | 99.71 | 100.09 | 99.57 | 99.04 | 98.66 | 99.50 | 99.99 | 98.77 |
| Fs | 27.0 | 40.7 | 50.1 | 59.2 | 67.7 | 80.8 | 56.0 | 64.1 | 70.7 | 19.3 | 28.3 | 43.4 | 46.9 | 53.6 | 53.2 |
| Wo | 12.0 | 15.3 | 11.3 | 13.1 | 15.8 | 9.0 | 23.6 | 19.0 | 11.3 | 33.0 | 30.4 | 31.0 | 37.2 | 33.8 | 41.5 |

n.d., not determined.

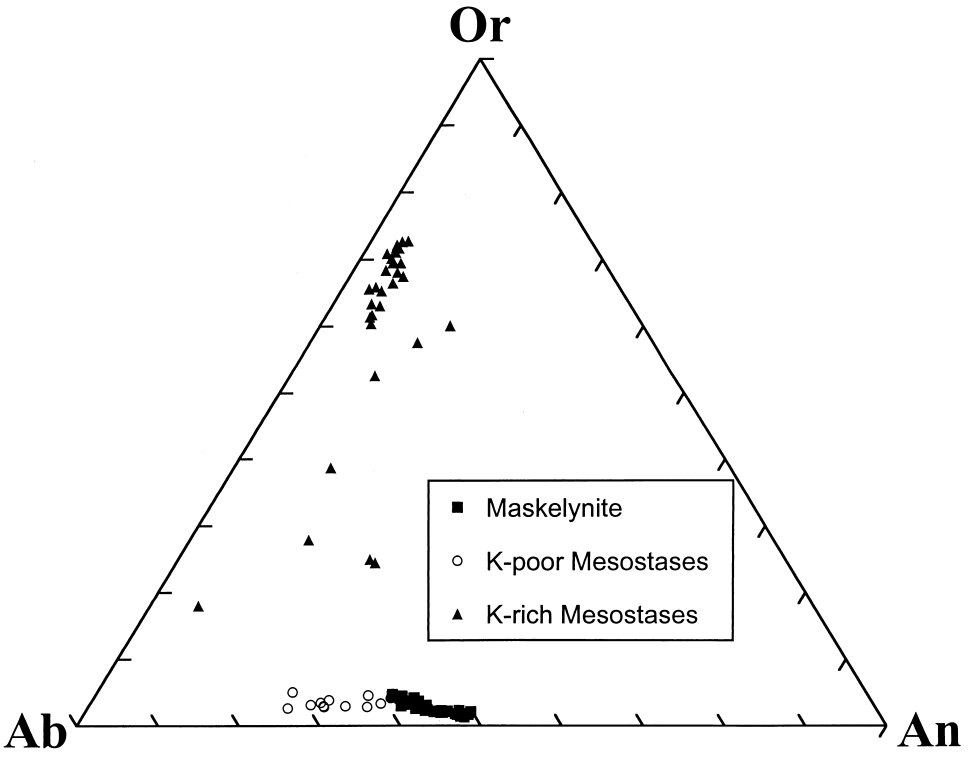


Fig. 7. Compositions of maskelynite, K-rich and K-poor mesostases from the dark, mottled lithology and its late-stage melt pockets. Maskelynite is slightly more albitic than in normal Zagami. Mesostases consist of feldspar + $SiO_2$ ± K-feldspar or shock-produced glasses of these compositions. The K-poor mesostasis is consistently more albitic than maskelynite.

mineralogies of the various lithologies and their modal abundances (Fig. 10). Petrographic (McCoy et al., 1992) and experimental (Stolper and McSween, 1979; McCoy and Lofgren, 1996) studies suggest that pigeonite was the liquidus phase. McCoy et al. (1992) suggested that augite co-crystallization commenced shortly afterwards, but ceased at ~15% crystallization of the bulk melt, at which time FeO-enrichment is observed in pigeonite rimming the homogeneous Mg-rich cores. McCoy et al. (1992) argued that this marked the point of eruption of the phenocryst-bearing lava flow, with augite crystallization commencing again, followed by plagioclase. For much of the crystallization history of Zagami, augite, pigeonite, and plagioclase were co-crystallizing. Physical segregation of early-formed, relatively magnesian pyroxene likely formed normal Zagami, possibly through processes such as crystal settling, melt migration, and flow differentiation. A break in augite compositions between the dark, mottled lithology and its late-stage melt pockets likely reflects cessation of augite crystallization and the onset of phosphate crystallization. This appears to have occurred after about 95 vol.% of the rock had crystallized (Fig. 10). During crystallization, P concentrated in the melt until it reached saturation and calcium phosphates began to crystallize. The melt was too poor in calcium to support crystallization of phosphates, plagioclase, pigeonite, and augite and, therefore, augite crystallization ceased. Plagioclase crystallization may well have been stabilized by Al in the melt. At ~98% crystallization, the melt became too FeO-rich to crystallize pigeonite and, instead, a fayalite-$SiO_2$ mixture formed. At this stage, much of the melt had crystallized and the melt pockets were isolated from each other. As noted previously, their crystallization histories were controlled by local compositional variabilities in the late-stage melts. In some pockets, sufficient P was present to allow for the crystallization of phosphates, producing the phosphate-bearing fayalite intergrowths. In other late-stage melts, the breakdown of pigeonite and the absence of sufficient P allowed augite to crystallize once again, producing the augite-bearing fayalite intergrowths. The final crystallization products are the mesostases and

Table 3. Representative analyses of maskelynite from the dark, mottled lithology and its late-stage melt pockets, illustrating the range of compositional variability.

| | Dark, mottled | | | Late-stage melt | |
|---|---|---|---|---|---|
| $SiO_2$ | 56.8 | 58.0 | 59.0 | 58.6 | 59.4 |
| $Al_2O_3$ | 26.4 | 25.9 | 25.1 | 25.3 | 24.9 |
| FeO | 0.78 | 0.72 | 1.04 | 0.63 | 0.79 |
| CaO | 9.98 | 9.25 | 7.95 | 8.42 | 7.90 |
| $Na_2O$ | 5.81 | 6.27 | 6.62 | 6.44 | 6.95 |
| $K_2O$ | 0.37 | 0.42 | 0.65 | 0.60 | 0.80 |
| Total | 100.18 | 100.57 | 100.39 | 99.99 | 100.74 |
| Ab | 50.2 | 53.8 | 57.9 | 56.0 | 58.8 |
| Or | 2.1 | 2.3 | 3.7 | 3.5 | 4.4 |

Table 4. Compositions of K-poor and K-rich mesostases from late-stage melt pockets in the dark, mottled lithology illustrating the range of compositions.

| | K-poor mesostases | | | | | K-Rich mesostases | | | | |
|---|---|---|---|---|---|---|---|---|---|---|
| $SiO_2$ | 58.7 | 59.7 | 78.3 | 78.8 | 97.6 | 98.3 | 74.5 | 77.9 | 77.4 | 76.9 |
| $Al_2O_3$ | 24.7 | 24.7 | 13.4 | 12.9 | 2.37 | 1.34 | 12.5 | 11.8 | 11.6 | 12.0 |
| FeO | 0.74 | 0.59 | 0.37 | 0.45 | 0.11 | 0.09 | 1.45 | 1.28 | 0.97 | 0.74 |
| CaO | 7.70 | 7.63 | 3.52 | 4.00 | 0.51 | 0.09 | 1.92 | 0.84 | 0.68 | 0.63 |
| $Na_2O$ | 7.23 | 6.74 | 4.53 | 4.03 | 0.84 | 0.59 | 2.34 | 1.83 | 1.80 | 1.67 |
| $K_2O$ | 0.62 | 0.84 | 0.30 | 0.29 | 0.04 | 0.22 | 7.04 | 7.28 | 7.49 | 8.16 |
| Total | 99.69 | 100.20 | 100.42 | 100.47 | 101.47 | 100.63 | 99.75 | 100.93 | 99.90 | 100.10 |
| Qz | 0 | 1.4 | 43.5 | 46.5 | 91.4 | 93.8 | 30.5 | 36.5 | 36.5 | 34.5 |
| Ab | 60.8 | 58.5 | 68.0 | 62.7 | 72.6 | 76.0 | 29.1 | 25.9 | 25.2 | 22.6 |
| An | 35.9 | 36.7 | 29.0 | 34.4 | 24.7 | 6.0 | 13.3 | 6.6 | 5.3 | 4.6 |
| Or | 3.4 | 4.8 | 3.0 | 2.9 | 2.9 | 18.0 | 57.6 | 67.5 | 69.5 | 72.7 |

See text for explanation of end member compositions.

opaque phases (e.g., pyrrhotite, Fe-Ti-oxides). Therefore, the late crystallization history of Zagami is largely controlled by the abundances of iron, calcium, and phosphorus.

The general picture, outlined above, of the crystallization history of Zagami is supported by the trace element microdistributions in minerals in the different lithologies (i.e., normal Zagami, the dark, mottled lithology and the late-stage melt pockets in the latter). The data presented here clearly indicate that these lithologies are related by progressive fractional crystallization. Most noteworthy is the similarity of the REE patterns of the same mineral in each of these lithologies (Fig. 8). It has been previously demonstrated that the REE patterns of melts in equilibrium with early- as well as late-formed minerals of the basaltic shergottites are parallel to the REE pattern of their respective bulk rocks, suggesting closed system fractional crystallization following some degree of crystal accumulation (Wadhwa et al., 1994; Lundberg et al., 1988). Therefore, the noted similarity of REE patterns of minerals between normal Zagami and the more highly evolved lithologies (data for which are presented here; Fig. 8) then implies that these lithologies are related by fractionation of the same parent magma. In addition, the fact that the incompatible trace element composition of pigeonites in the dark, mottled lithology and in the largest of the late-stage melt pockets overlaps that of normal Zagami, and extends to higher concentrations than in the latter (Fig. 9) supports progressive fractional crystallization to produce the dark, mottled lithology and the late-stage melt pockets, following the formation and segregation of minerals comprising normal Zagami from the parent magma. Finally, the higher abundances of REEs in phosphates of the dark, mottled lithology compared to normal Zagami also point towards a more evolved composition for the latter. However, one may note that although the REE concentrations in whitlockite of the largest late-stage melt pocket are, on average, higher than that in normal Zagami, they fall within the range of REE abundances found in whitlockites of the dark, mottled lithology. We suggest that this may be due to the local variability in the composition (particularly, the phosphorous content, which would determine when the whitlockite began crystallization and, therefore, the REE content this mineral would incorporate) of the melt from which this melt pocket formed, relative to the average composition that formed the dark, mottled lithology.

The idea that the bulk compositions of Shergotty and Zagami are not melt compositions, but record some degree of crystal

Table 5. Representative analyses of whitlockite and apatite from late-stage melt pockets in the dark, mottled lithology illustrating the range of compositional variability.

| | Whitlockite | | | | Apatite | | |
|---|---|---|---|---|---|---|---|
| $SiO_2$ | 0.10 | 0.07 | 0.10 | 0.11 | 0.50 | 0.44 | 0.69 |
| FeO | 3.09 | 3.89 | 4.96 | 5.15 | 0.78 | 0.94 | 1.12 |
| MnO | 0.11 | 0.18 | 0.22 | 0.22 | 0.14 | 0.15 | 0.10 |
| MgO | 1.97 | 1.65 | 0.85 | 0.59 | 0.07 | 0.06 | n.d. |
| CaO | 47.1 | 47.1 | 46.7 | 46.8 | 53.4 | 54.2 | 53.1 |
| $Na_2O$ | 1.14 | 1.20 | 1.22 | 1.17 | b.d. | b.d. | n.d. |
| $P_2O_5$ | 44.7 | 44.7 | 45.3 | 44.8 | 40.7 | 40.1 | 41.2 |
| F | b.d | b.d | b.d. | b.d. | 1.12 | 1.25 | 1.27 |
| Cl | b.d. | b.d. | b.d. | b.d. | 2.92 | 3.04 | 2.36 |
| Total | 98.21 | 98.79 | 99.35 | 98.84 | 99.63 | 100.18 | 99.84 |
| O≡F,Cl | — | — | — | — | 1.12 | 1.22 | 1.20 |
| Total | — | — | — | — | 98.51 | 98.96 | 98.64 |

n.d., not determined; b.d., below detection.

Table 6. Compositions of fayalite in late-stage melt pockets in the dark, mottled lithology illustrating the range of compositional variability.

| | (1) | (2) | (3) | (4) | (5) |
|---|---|---|---|---|---|
| $SiO_2$ | 30.2 | 28.9 | 29.3 | 29.4 | 29.5 |
| FeO | 64.6 | 67.3 | 68.4 | 68.2 | 66.8 |
| MnO | 1.84 | 1.86 | 1.91 | 1.87 | 1.76 |
| MgO | 4.01 | 1.52 | 1.22 | 1.30 | 2.31 |
| CaO | 0.37 | 0.42 | 0.33 | 0.44 | 0.24 |
| Total | 101.02 | 100.00 | 101.16 | 101.21 | 100.61 |
| Fa | 90.0 | 96.1 | 96.5 | 96.7 | 90.9 |

(1),(2) In augite-bearing fayalite intergrowth, (3) In Phosphate-bearing fayalite intergrowth, (4) In whitlockite, (5) In Fe, Ti-oxide n.d., not determined; b.d., below detection.

Table 7. Representative analyses of ilmenite and titanomagnetite in the three lithologies of Zagami illustrating the range of compositional variability.

| | Normal Zagami | | Dark, mottled lithology | | Late-stage melt pockets | |
|---|---|---|---|---|---|---|
| | (1) | (2) | (1) | (2) | (1) | (2) |
| $TiO_2$ | 49.7 | 22.1 | 50.2 | 24.4 | 50.3 | 24.3 |
| $Al_2O_3$ | 0.09 | 2.76 | 0.08 | 1.89 | 0.07 | 2.22 |
| $Cr_2O_3$ | 0.15 | 2.16 | 0.21 | 1.56 | b.d. | b.d. |
| MgO | 0.82 | 0.44 | 0.92 | 0.74 | 0.19 | 0.14 |
| FeO | 47.3 | 70.8 | 47.1 | 69.4 | 47.8 | 71.5 |
| MnO | 0.71 | 0.56 | 0.64 | 0.64 | 0.75 | 0.64 |
| Total | 98.77 | 98.82 | 99.15 | 98.63 | 99.11 | 98.8 |

(1) Ilmenite, (2) Titanomagnetite; b.d. = below detection limits.

accumulation was suggested by Stolper and McSween (1979). More recently, several authors (e.g., Harvey et al., 1996; McSween et al., 1996; Mikouchi et al., 1996) have suggested that QUE 94201 may represent a melt composition unaffected by crystal accumulation. With these new lithologies in Zagami, we have, for the first time, sampled both crystal cumulates and residual melts in a single rock, allowing us to better constrain the bulk composition of this magma. A perplexing feature of shergottites is that although the homogeneous, Mg-rich cores in Shergotty and Zagami comprise only 10–20% of the rocks (McCoy et al., 1992), crystallization experiments on bulk compositions of these rocks produce 35–45% pyroxene having the composition of the Mg-rich cores (Stolper and McSween, 1979; McCoy and Lofgren, 1996; Hale et al., 1998). Rather than completely reflecting crystal accumulation, as suggested by Stolper and McSween (1979), this may reflect the fact that the actual bulk composition from which Zagami crystallized differs substantially from the normal Zagami lithology used by Stolper and McSween (1979) and McCoy and Lofgren (1996). Using data from these experiments, we calculate a $K_D$ for FeO in the first crystallizing pigeonite of ~0.76. This would suggest that the natural magnesian pyroxenes (~$Fs_{30}$) might form as the first crystallizing phase from a magma with ~24.7 wt.% FeO. By comparison, the bulk composition of normal Zagami contains only 18.2 wt.% FeO (McCoy et al., 1992). Additionally, even the intercumulus melt (the bulk composition without the Mg-rich pyroxene cores) contained only 18.5 wt.% FeO (McCoy et al., 1992). However, a bulk composition based on mineral abundances in the various lithologies (Table 1), mineral compositions (McCoy et al., 1992; McCoy, unpublished data; this work) and estimates of the abundances of the various lithologies would contain ~19.1 wt.% FeO. This value should be considered a minimum FeO concentration for the true bulk composition from which Zagami crystallized, because the FeO-rich lithologies may be substantially more abundant in the magma body than observed in the main mass of this meteorite. This suggests that crystallization experiments using an FeO-enriched composition would produce fewer magnesian pyroxenes and might explain some of the discrepancies between experimental and petrologic studies.

An interesting feature of these late-stage magmatic lithologies (i.e., the dark, mottled lithology and the melt pockets) is the near-absence of structurally-bound water. If the Zagami parent magma had contained any water, one might expect the late-stage crystallization products such as apatite to be enriched

Table 8. Representative rare earth element abundances (in ppm) in minerals in the dark, mottled lithology and the late-stage melt pockets. Numbers in parentheses are 1$\sigma$ errors (from counting statistics only) in the last significant digits.

| | Dark, mottled lithology | | | | | Late-stage melt pockets | | | | | |
|---|---|---|---|---|---|---|---|---|---|---|---|
| | Pigeonite | Augite | Maskelynite | Apatite | Whitlockite | Pigeonite | Augite | Maskelynite | Fayalite | Apatite | Whitlockite |
| La | 0.015 (2) | 0.052 (7) | 0.109 (4) | 3.7 (2) | 130 (2) | 0.014 (3) | 0.081 (8) | 0.050 (4) | b.d. | 5.4 (4) | 132 (2) |
| Ce | 0.049 (4) | 0.21 (2) | 0.211 (8) | 11.2 (4) | 314 (4) | 0.056 (8) | 0.38 (4) | 0.081 (7) | b.d. | 16.9 (9) | 314 (4) |
| Pr | 0.012 (2) | 0.036 (6) | 0.024 (2) | 1.4 (1) | 40 (1) | 0.014 (3) | 0.083 (7) | 0.008 (1) | b.d. | 2.5 (2) | 40 (1) |
| Nd | 0.066 (7) | 0.32 (3) | 0.074 (4) | 8.1 (3) | 202 (4) | 0.09 (1) | 0.69 (3) | 0.026 (4) | b.d. | 12.8 (5) | 208 (4) |
| Sm | 0.047 (7) | 0.23 (3) | 0.016 (3) | 2.9 (2) | 75 (3) | 0.076 (11) | 0.36 (3) | 0.014 (4) | b.d. | 4.3 (4) | 72 (3) |
| Eu | 0.015 (2) | 0.079 (8) | 0.50 (2) | 1.0 (1) | 23 (1) | 0.027 (3) | 0.11 (1) | 0.40 (3) | b.d. | 1.2 (1) | 18 (1) |
| Gd | 0.11 (1) | 0.42 (5) | 0.023 (3) | 4.1 (3) | 105 (4) | 0.15 (2) | 0.89 (7) | 0.013 (4) | b.d. | 6.2 (7) | 91 (4) |
| Tb | 0.024 (3) | 0.093 (14) | 0.004 (1) | 0.71 (6) | 19 (1) | 0.046 (8) | 0.20 (2) | 0.002 (1) | 0.007 (3) | 1.1 (1) | 18 (1) |
| Dy | 0.27 (1) | 0.78 (5) | 0.019 (2) | 5.4 (2) | 139 (3) | 0.45 (3) | 1.74 (6) | b.d. | 0.073 (10) | 7.3 (4) | 128 (3) |
| Ho | 0.060 (6) | 0.14 (2) | b.d. | 1.0 (1) | 28 (1) | 0.09 (1) | 0.43 (3) | b.d. | 0.038 (6) | 1.5 (1) | 28 (1) |
| Er | 0.23 (1) | 0.44 (3) | b.d. | 2.9 (1) | 83 (2) | 0.43 (2) | 1.37 (5) | b.d. | 0.13 (1) | 3.0 (2) | 67 (2) |
| Tm | 0.034 (5) | 0.073 (12) | b.d. | 0.39 (3) | 11 (1) | 0.071 (1) | 0.18 (1) | b.d. | 0.045 (6) | 0.40 (4) | 10 (1) |
| Yb | 0.26 (1) | 0.51 (4) | b.d. | 2.4 (1) | 75 (3) | 0.59 (5) | 1.47 (6) | b.d. | 0.52 (3) | 2.2 (2) | 50 (2) |
| Y | 1.62 (7) | 3.99 (18) | 0.058 (4) | 33.4 (6) | 961 (5) | 3.32 (11) | 8.58 (16) | 0.030 (3) | 0.76 (4) | 31.2 (9) | 568 (4) |

b.d. = below detection limit of the ion microprobe.

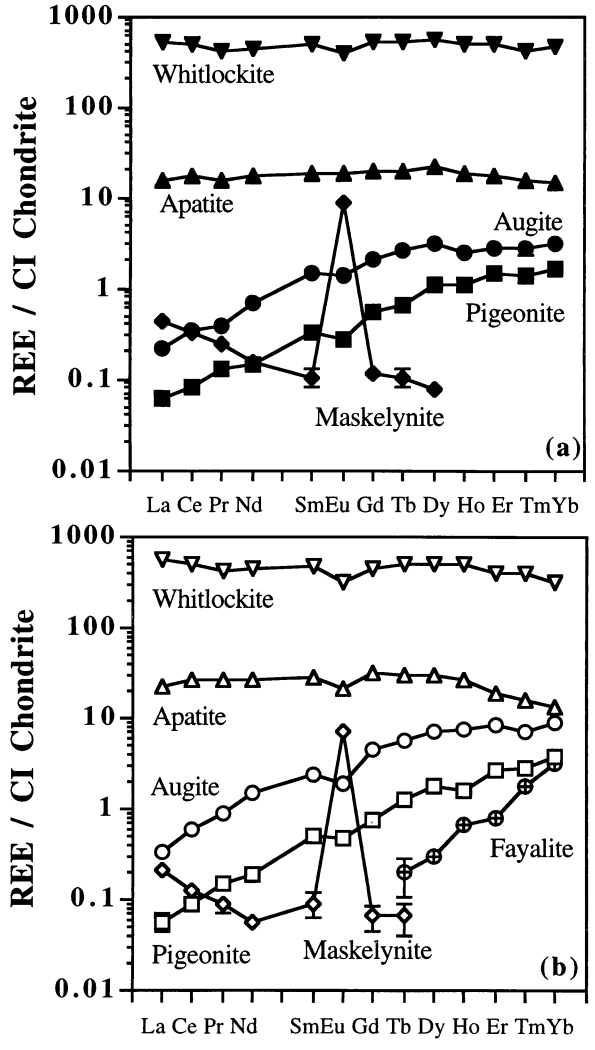


Fig. 8. Representative REE abundances (normalized to CI values of Palme et al., 1981) in minerals of (a) dark, mottled lithology and (b) the largest of the late-stage melt pockets. HREE abundances in maskelynite and LREE abundances in fayalite are not shown because they are below the detection limit of the ion microprobe. Error bars are $1\sigma$ from counting statistics only; in cases where error bars cannot be seen, they are smaller than the data points.

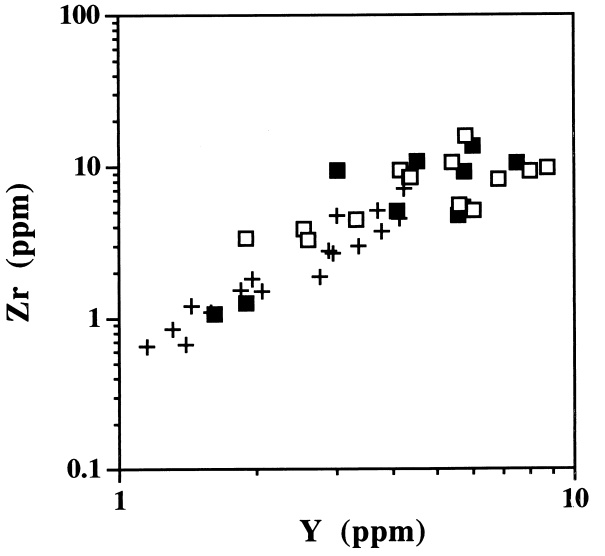


Fig. 9. Zr vs. Y abundances in pigeonites of normal Zagami (crosses; data from Wadhwa et al., 1994), dark, mottled lithology (filled squares) and the largest of the late-stage melt pockets (open squares). Note that the x- and y-axes are plotted on logarithmic scales.

in their hydrous component. However, apatite, which comprises <0.5 wt.% of the largest, late-stage melt pocket and contains ~0.5 wt.% water, accounts for less than 25 ppm water in this highly evolved lithology. Because one of the most evolved lithologies in Zagami is so dry, the melt from which it crystallized must also have been extremely dry. This does not solve the more interesting problem of whether the original magma was dry, as one might infer from the work of Watson et al. (1994) and Popp et al. (1995a, b), or if it experienced significant devolatilization during its emplacement history prior to crystallization, as has been suggested by McSween and Harvey (1993). However, the inference of an extremely dry magma at the time of crystallization suggests that if degassing did occur, it must have been an extremely efficient process.

Schaber et al. (1978) demonstrated that 10-m thick flows are extremely common in the Tharsis region of Mars and comparably thick near-surface intrusives must also be abundant. Since Zagami may have crystallized from a flow of similar thickness, it may be that rocks with multiple lithologies like those in Zagami are fairly common on Mars. While evidence for large-scale differentiation of basalts has been observed (e.g., Mustard et al., 1997), future missions might expect to find compositional differentiation within most magma units on Mars.

## 5. CONCLUSIONS

Zagami experienced a prolonged history of fractional crystallization, producing a variety of lithologies which are increasingly enriched in FeO and incompatible elements (e.g., P, Ti, Zr, REEs).

The bulk composition of the magma unit from which Zagami formed is likely to be significantly more FeO-rich than previously assumed. This may partially explain discrepancies in the magmatic history derived from petrologic and experimental studies.

The magma from which Zagami crystallized was remarkably dry, with the most evolved lithology containing ~25 ppm of

Table 9. Parameters indicating that the sequence of normal Zagami to the dark, mottled lithology to the late-stage melt pockets is a sequence of increasing fractional crystallization, resulting in the formation of increasingly evolved residual melts.

| | Normal Zagami | Dark, mottled lithology | Late-stage melts |
|---|---|---|---|
| Fa intergrowth (wt.%) | 0.0 | Trace | 39.9 |
| Fs in pigeonite | 28.7–54.3 | 27.0–80.8 | 56.0–70.7 |
| Y in pigeonite (ppm) | 1.1–4.2 | 1.6–7.5 | 2.0–8.8 |
| Ab in maskelynite | 42–53 | 50.2–58.8 | 56.0–58.8 |
| FeO in whitlockite (wt.%) | 2.6–3.5 | 3.1–5.2 | 5.0–5.2 |

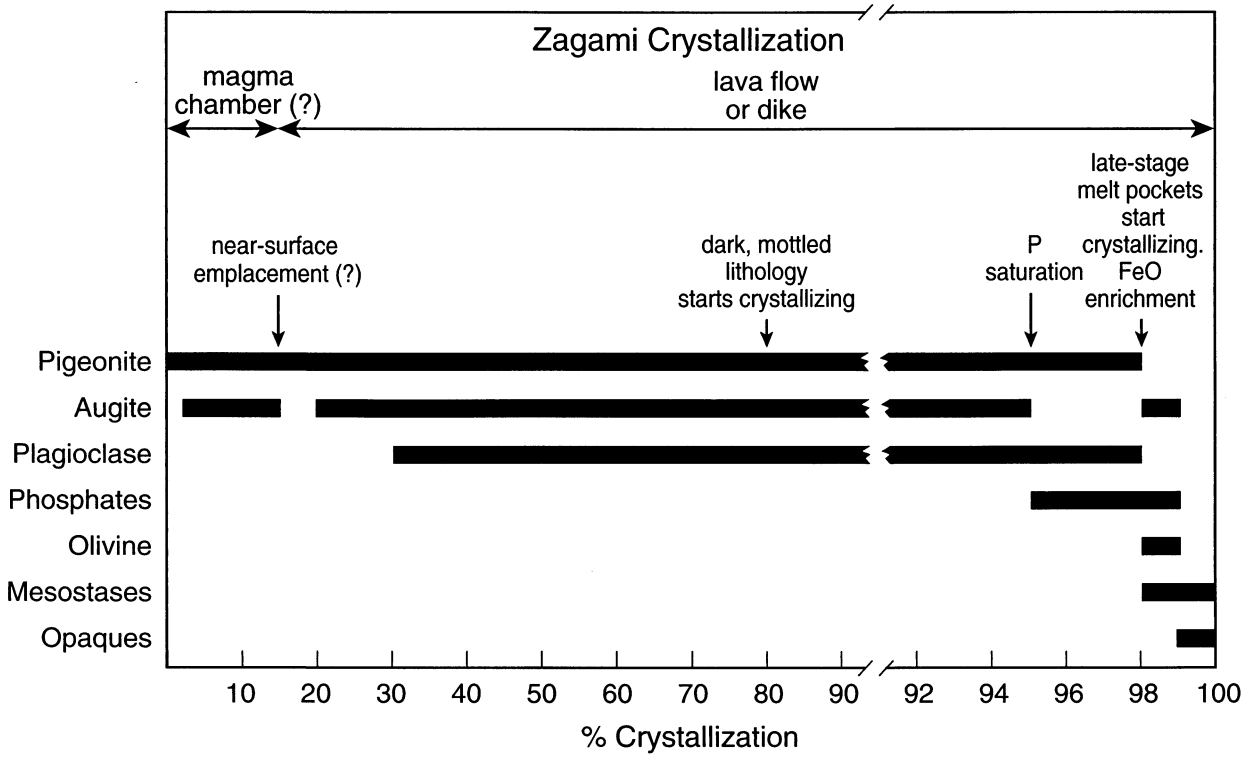


Fig. 10. The crystallization sequence in Zagami. Bars represent appearance and disappearance of various phases. The x-axis gives approximate percent crystallization of the melt for major changes in the crystallization behavior, deduced from modes of Zagami.

structurally-bound water. It is unclear whether the magma was dry at the time of its formation or experienced extremely efficient outgassing prior to crystallization.

Differentiation of magma units at or near the surface of Mars may be a fairly common process and products of this differentiation may be expected while sampling magma units during future Mars missions.

*Acknowledgments*—Samples and thin sections were generously made available by L. Vistisen and D. Petersen (Niels Bohr Institute, Copenhagen), M. B. Madsen (H. C. Ørsted Institute, Copenhagen), R. Haag (Tucson, AZ), G. J. MacPherson (Smithsonian Institution) and A. J. Brearley (University of New Mexico). We particularly thank the first three colleagues for bringing these highly-evolved lithologies to our attention and spurring our renewed interest in Zagami. Helpful discussions and assistance by G. J. Taylor and L. Leshin are appreciated. Expert technical assistance was provided by T. Servilla, T. Hulsebosch, D. McGee, T. Tatnall, P. Bernhard, V. Yang, and S. Wentworth. Substantive reviews by H. Y. McSween, Jr. and L. A. Leshin substantially improved and clarified the paper. Financial support was provided by a National Research Council Postdoctoral Fellowship at NASA Johnson Space Center (T. J. M.), NASA grants NAGW-3281 and NAG 5-4212 (K. Keil, PI) and NAG-9-55 (G. Crozaz, PI). This is Hawaii Institute of Geophysics and Planetology publication no. 1028 and School of Ocean and Earth Science and Technology publication no. 4732.

## REFERENCES

Brearley A. J. (1991) Subsolidus microstructures and cooling history of pyroxenes in the Zagami shergottite. *Lunar Planet. Sci.* **22,** 135–136 (abstr.).

Darot M. (1973) Methodes d'analyse structurale et cinematique. Application a'letude du massif ultrabasique de la Sierra Ronda. Ph.D. dissertation, Univ. Nantes.

Hale V. P. S., McSween H. Y. Jr., and McKay G. (1998) Cumulus pyroxene in Shergotty: Why do estimates vary between experimental and observational studies? *Lunar Planet. Sci.* **29,** 1109 (abstr.).

Harvey R. P., McCoy T. J., and Leshin L. A. (1996) Shergottite QUE 94201: Texture, mineral compositions, and comparison with other basaltic shergottites. *Lunar Planet. Sci.* **27,** 497–498 (abstr.).

Lundberg L. L., Crozaz G., McKay G., and Zinner E. (1988) Rare earth element carriers in the Shergotty meteorite and implications for its chronology. *Geochim. Cosmochim. Acta* **52,** 2147–2163.

Marti K., Kim J. S., Thakur A. N., McCoy T. J., and Keil K. (1995) Signatures of the Martian atmosphere in glass of the Zagami meteorite. *Science* **267,** 1981–1984.

McCoy T. J., Taylor G. J., and Keil K. (1992) Zagami: Product of a two-stage magmatic history. *Geochim. Cosmochim. Acta* **56,** 3571–3582.

McCoy T. J., Keil K., and Taylor G. J. (1993) The dregs of crystallization in Zagami. *Lunar Planet. Sci.* **24,** 947–948 (abstr.).

McCoy T. J., Wadhwa M., and Keil K. (1995) Zagami: Another new lithology and a complex near-surface magmatic history. *Lunar Planet. Sci.* **26,** 925–926 (abstr.).

McCoy T. J., and Lofgren G. E. (1996) The crystallization of the Zagami shergottite: A 1 atm. experimental study. *Lunar Planet. Sci.* **27,** 839–840 (abstr.).

McSween H. Y. Jr., and Harvey R. P. (1993) Outgassed water on Mars: Constraints from melt inclusions in SNC meteorites. *Science* **259,** 1890–1892.

McSween H. Y. Jr. and Jarosewich E. (1983) Petrogenesis of the Elephant Moraine A79001 meteorite: Multiple magma pulses on the shergottite parent body. *Geochim. Cosmochim. Acta* **47,** 1501–1513.

McSween H. Y. Jr., Eisenhour D. D., Taylor L. A., Wadhwa M., and

Crozaz G. (1996) QUE 94201 shergottite: Crystallization of a Martian basaltic magma. *Geochim. Cosmochim. Acta* **60,** 4563–4569.

Mikouchi T., Miyamoto M., and McKay G. A. (1996) Mineralogy and petrology of new Antarctic shergottite QUE 94201: A coarse-grained basalt with unusual pyroxene zoning. *Lunar Planet. Sci.* **27,** 879–880 (abstr.).

Mustard J. F., Murchie S., Erard S., and Sunshine J. (1997) In situ compositions of Martian volcanics: Implications for the mantle. *J. Geophys. Res.-Planets* **102,** 25,605–25,625.

Palme H., Suess H., and Zeh H. D. (1981) Abundances of elements in the solar system. In *Landolt-Börnstein*; *Astronomy and Astrophysics*, Vol. 2a, pp. 257–272. Springer-Verlag.

Popp R. K., Virgo D., Yoder H. S. Jr., Hoering T. C., and Phillips M. W. (1995a) An experimental study of phase equilibria and Fe oxy-component in kaersutitic amphibole: Implications for the $f_{H2}$ and $a_{H_2O}$ in the upper mantle. *Am. Min.* **80,** 534–548.

Popp R. K., Virgo D., and Phillips M. W. (1995b) H deficiency in kaersutitic amphiboles: Experimental verification. *Am. Min.* **80,** 1347–1350.

Schaber G. G., Horstman K. C., and Dial A. L. Jr. (1978) Lava flow materials in the Tharsis region of Mars. *Proc. 9th Lunar Planet. Sci. Conf.*, 3433–3458.

Stolper E., and McSween H. Y. Jr. (1979) Petrology and origin of the shergottite meteorites. *Geochim. Cosmochim. Acta* **43,** 1475–1498.

Treiman A. H., and Sutton S. R. (1992) Petrogenesis of the Zagami meteorite: Inferences from synchrotron X-ray (SXRF) microprobe and electron microprobe analyses of pyroxenes. *Geochim. Cosmochim. Acta* **56,** 4059–4074.

Vistisen L., Petersen D., and Madsen M. B. (1992) Mössbauer spectroscopy showing large-scale inhomogeneity in the presumed Martian meteorite Zagami. *Physica Scripta* **46,** 94–96.

Wadhwa M., McCoy T. J., Keil K., and Crozaz G. (1993) The chemical and physical evolution of late-stage melt in Zagami. *Meteoritics* **28,** 453 (abstr.).

Wadhwa M., McSween H. Y. Jr., and Crozaz G. (1994) Petrogenesis of shergottite meteorites inferred from minor and trace element microdistributions. *Geochim. Cosmochim. Acta* **58,** 4213–4229.

Watson L. L., Hutcheon I. D., Epstein S., and Stolper E. M. (1994) Water on Mars: Clues from deuterium/hydrogen and water contents of hydrous phases in SNC meteorites. *Science* **265,** 86–90.

Zinner E., and Crozaz G. (1986) A method for the quantitative measurement of rare earth elements in the ion microprobe. *Intl. J. Mass Spectrom. Ion Proc.* **69,** 17–38.